Advances in Bridge Engineering

ORIGINAL INNOVATION

Open Access

Damping effects of a stay cable attached with a viscous damper and a high damping rubber damper considering cable bending stiffness and damper support flexibility

Duy Thao Nguyen[1*], Si Quanh Chau[2] and Hoang Nam Phan[1]

*Correspondence:
ndthao@dut.udn.vn

[1] Faculty of Road and Bridge Engineering, The University of Danang–University of Science and Technology, Danang 550000, Vietnam
[2] Faculty of Bridge and Road, Danang Architecture University, Danang 550000, Vietnam

Abstract

To mitigate cable oscillations in cable-stayed bridges, a common approach involves using a strategically positioned viscous damper near the cable's anchorage and bridge deck. However, for longer cables, this method may be insufficient due to installation constraints. In such cases, supplementing the damping system with a high-damping rubber (HDR) damper near the cable's anchorage point on the bridge tower becomes imperative to enhance the cable's damping ratio. Conventional designs often overlook crucial factors like viscous damper support stiffness and stay cable bending stiffness when integrating dampers into cable-stayed structures. This study presents findings on achieving an effective damping ratio in stay cables by using both a viscous damper and an HDR damper, considering the influence of viscous damper support stiffness and stay cable bending stiffness. The results indicate that the combined deployment of these dampers achieves a damping efficiency approximately equivalent to the sum of their individual effects. Importantly, decreased viscous damper support stiffness significantly affects the damping effectiveness, leading to a rapid decline in the stay cable's damping ratio. While stay cable bending stiffness also influences the damping ratio, its impact is relatively less pronounced than that of viscous damper support stiffness. The study outcomes enable a more accurate prediction of the achievable damping ratio for a stay cable with additional components, considering both damper support stiffness and stay cable bending stiffness. Furthermore, the study explores parameters of both the viscous damper and HDR damper, such as the viscous coefficient, loss coefficient, HDR damper stiffness, and damper placement, evaluating their influence on the first damping ratio of the stay cable. The survey results provide valuable insights for determining optimal parameters for both dampers, maximizing the damping efficiency of cable-stayed bridges.

Keywords: Viscous damper, Cable damping ratio, High-damping rubber damper, Viscous damper support stiffness, Bending stiffness

1 Introduction

Stay cables serve as the primary load-bearing elements in cable-stayed bridges and are characterized by their notably low damping ratio, making them structurally flexible in the horizontal plane (Abdel-Ghaffar and Khalifa 1991; Javanmardi et al. 2022). Throughout their operational lifespan, these stay cables are susceptible to oscillations induced by a variety of external forces, including wind-induced vibrations (Matsumoto et al. 2001, 2003; Kumarasena et al. 2005; Fujino et al. 2014; Hung and Thao 2020a; Nguyen et al. 2022), the combined effects of rain and wind (Gu 2009; Vo et al. 2016; Hung and Thao 2020b), and dynamic loads applied to the bridge (de Sá Caetano 2007). To effectively mitigate these oscillations, engineers often employ mechanical dampers, including viscous dampers (Pacheco et al. 1993; Main 2002; Main and Jones 2002a, b; Nielsen and Krenk 2003) and high-damping rubber (HDR) dampers (Jones 1967; Nakamura et al. 1998; Fujino and Hoang 2008; Cu and Han 2015; Le et al. 2020).

Traditionally, these dampers are affixed to the stay cables, strategically positioned near the attachment points on the bridge deck. This placement is driven by considerations of aesthetics and maintenance convenience, but it tends to limit their impact to a relatively short section of the cable's overall length, thereby reducing their effectiveness. Furthermore, the damping ratio of stay cables with these dampers depends on a complex interplay of cable and damper parameters. To accurately predict the damping ratio of a stay cable equipped with a damper, extensive study has explored various cable parameters. This includes an in-depth examination of factors such as the influence of cable bending stiffness (Main and Jones 2007; Fujino and Hoang 2008), cable sag (Nielsen and Krenk 2003; Wang et al. 2005; Fujino and Hoang 2008), and cable inclination angle (Sun and Huang 2008; Fujino and Hoang 2008). Study efforts have also delved into the numerous influences stemming from damper parameters, encompassing an assessment of the damper's internal stiffness (Zhou and Sun 2006; Beskhyroun et al. 2011), the nonlinear viscosity coefficient of the damper (Main and Jones 2002b; Sun et al. 2019), the stiffness properties of the viscous damper support (Sun and Huang 2008; Fujino and Hoang 2008), and considerations related to the mass of the damper (Duan et al. 2019a, b). Many studies examining the effects of cable and damper parameters on the cable's damping forces, as previously mentioned, have focused on cable systems with a single damper. However, in the context of cable-stayed bridges with expansive spans, exemplified by prominent structures like the Tatara Bridge in Japan or the Stonecutters Bridge in Hong Kong, where the lengths of stay cables exceed an impressive 300 m, achieving the required damping ratio with just one damper presents a significant challenge. In response to this challenge, the proposal to install two dampers strategically positioned at different locations has emerged as an appealing and practical solution (Zhou and Sun 2006; Caracoglia and Jones 2007; Sun and Chen 2015; Chen et al. 2020; Di et al. 2021; Wang et al. 2022; Liu et al. 2023).

An exploration into the impact of attaching two viscous dampers on the damping ratio of stay cables revealed that when two viscous dampers are closely positioned on the same side of the cable's end, there is no significant enhancement in the damping ratio of the stay cable (Caracoglia and Jones 2007). Conversely, attaching two viscous dampers at two separate locations on opposite sides of the cable's end can substantially increase the maximum attainable damping ratio of the stay cable. Similar study results were corroborated by Hoang

and Fujino (2008). Furthermore Nguyen and Vo (2020b) conducted a study aimed at determining the damping ratio of stay cables when two HDR devices were incorporated. Di et al. (2020) presented study results that illustrate the augmentation of the damping ratio of stay cables through the utilization of both a viscous damper and a damping rubber damper. To streamline analytical models, most studies evaluating the damping ratio of stay cables with two dampers often omit the consideration of the cable's bending stiffness. In studies undertaken by the author concerning stay cables outfitted with two HDR dampers (Nguyen et al. 2021), and two friction dampers (Nguyen and Vo 2020a), it was observed that an increase in the cable's bending stiffness significantly changes the damping ratio of the stay cable.

Building upon the groundwork laid by the author in previous studies (Nguyen and Vo 2020a; Nguyen et al. 2021), this study aims to introduce a comprehensive theoretical model, which is designed to rigorously assess the damping ratio of stay cables, taking into consideration the presence of both a viscous damper and an HDR damper. Notably, the present model accounts for the viscous damper support stiffness and the bending stiffness of the stay cable, thus providing a more accurate representation of real-world scenarios. To enhance the model's practicality, the viscous damper support stiffness is translated into an equivalent viscosity coefficient for the viscous damper. The analytical results presented in this paper undergo meticulous cross-referencing and validation against findings published by researchers from previous works (Kumarasena et al. 2005; Fujino and Hoang 2008; Hoang and Fujino 2008; Cu and Han 2015).

The analysis explores the influence of various parameters associated with both dampers on the damping ratio of the stay cable, encompassing the viscosity coefficient, stiffness, loss factor, attachment location, and viscous damper support stiffness. Emphasizing the substantial impact of the latter, a decrease in its stiffness results in a noteworthy reduction in the damping ratio. In cable-stayed bridges with extensive spans, epoxy resin is commonly used to shield stay cables, enhancing their bending stiffness. The study scrutinizes the effect of bending stiffness on the damping ratio, revealing that, generally, for long-span stay cables, an increase in bending stiffness leads to a significant improvement.

The results enable a more accurate prediction of the maximum damping ratio for the stay cable, considering both a viscous damper and an HDR damper. This consideration, incorporating the support stiffness of the viscous damper and the bending stiffness of the stay cable, provides significant advantages over conventional designs. The study further investigates a three-way relationship involving the first damping ratio, attachment location, and viscosity coefficient of the viscous damper, extending to relationships with the viscous damper support stiffness and the HDR damper's spring factor and loss coefficient. Survey results facilitate determining optimal parameters for the viscosity damper, including its viscosity coefficient and attachment location, as well as optimal parameters for the HDR damper, such as the loss coefficient and rubber stiffness. Identifying these parameters is crucial for achieving the maximum damping effect in stay cables.

2 Methodology

2.1 Computational model and vibration equations for a stay cable equipped with a viscous damper and an HDR damper

Examining a scenario involving a stay cable under tension force denoted as S, the configuration to be explored involves attaching both a viscous damper and an HDR

damper to this cable, as visually presented in Fig. 1. In this context, the x-coordinate axis is defined to align itself parallel to the stay cable's longitudinal axis. The viscous damper is securely connected to the cable at position l_1, whereas the HDR damper is fastened at position l_2. The viscous damper support exhibits a degree of stiffness, denoted as K_S. Regarding the cable's inherent characteristics, it possesses an overall length of L and a unit mass, symbolized as m. For the sake of analytical simplicity, it is assumed that any minor frictional interactions between the cable and the surrounding air can be disregarded. Additionally, there is the presumption that the tensile forces experienced within the cable are significantly greater than the gravitational forces acting on the stay cable itself, the rotational stiffness at both ends of the stay cable is relatively small and can be neglected. To elucidate the dynamic behavior of this intricate system comprehensively, reference is made to established works, specifically sources (Fujino and Hoang 2008; Hoang and Fujino 2008; Nguyen et al. 2021). Drawing insights from the conclusions of these sources, an equation governing the transverse oscillations observed in this stay cable, characterized by the presence of two attached dampers, is derived. Importantly, this equation considers the stay cable's bending stiffness, denoted as EJ, and is mathematically expressed as

$$m\frac{\partial^2 u(x,t)}{\partial t^2} + EJ\frac{\partial^4 u(x,t)}{\partial x^4} - S\frac{\partial^2 u(x,t)}{\partial x^2} = f_1(x,t)\delta(x-l_1) + f_2(x,t)\delta\left(x-l_2^*\right), \quad (1)$$

where $\delta\left(x-l_j\right)(j=1,2)$ represents the Dirac delta function, C stands for the viscosity coefficient of the viscous damper, K_D represents the spring factor of the HDR damper, λ is the loss coefficient of the HDR damper, and $f_1(x,t)$ and $f_2(x,t)$ refer to the respective damping forces of the viscous damper and the HDR damper. At the point where the viscous damper is attached, the viscous damper support stiffness K_S is converted into an equivalent viscosity coefficient C_{eq} as

$$f_1(x,t) = C_{eq}\frac{\partial u(l_1,t)}{\partial t}, \text{with} \quad C_{eq} = \frac{C}{1+i\eta\frac{C}{K_S}}. \quad (2)$$

At the point where the HDR damper is attached,

$$f_2(x,t) = K_D(1+i\lambda)u\left(l_2^*,t\right), \quad (3)$$

where i stands for an imaginary unit ($i^2=-1$); η signifies the oscillation frequency of the stay cable.

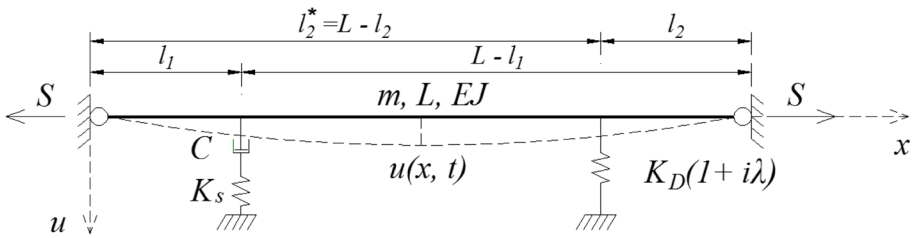

Fig. 1 Computational model of a stay cable with a viscous damper and an HDR damper

By employing the Fourier variable separation method, the solution to Eq. (1) takes the form,

$$u(x,t) = X(x)T(t). \tag{4}$$

Applying boundary conditions at the cable anchor positions, the continuity conditions, and balancing conditions for vertical forces at the damper attachment points as

$$\begin{cases} X(0) = X(L) = 0 \\ X^{"}(0) = X^{"}(L) = 0 \end{cases}, \tag{5a}$$

$$\begin{cases} X(l_1) = X\left(l_1^{+}\right) = X\left(l_1^{-}\right) \\ X\left(l_2^{*}\right) = X\left(l_2^{*+}\right) = X\left(l_2^{*-}\right) \end{cases}, \tag{5b}$$

$$\begin{cases} S\left(\left.\frac{\partial u}{\partial x}\right|_{x=l_1^{+}} - \left.\frac{\partial u}{\partial x}\right|_{x=l_1^{-}}\right) + EJ\left(\left.\frac{\partial^3 u}{\partial x^3}\right|_{x=l_1^{+}} - \left.\frac{\partial^3 u}{\partial x^3}\right|_{x=l_1^{-}}\right) = C_{eq}\frac{\partial u(l_1,t)}{\partial t} \\ S\left(\left.\frac{\partial u}{\partial x}\right|_{x=l_2^{*+}} - \left.\frac{\partial u}{\partial x}\right|_{x=l_2^{*-}}\right) + EJ\left(\left.\frac{\partial^3 u}{\partial x^3}\right|_{x=l_2^{*+}} - \left.\frac{\partial^3 u}{\partial x^3}\right|_{x=l_2^{*-}}\right) = K_D(1+i\lambda)u\left(l_2^{*},t\right) \end{cases}. \tag{5c}$$

After transformation, it becomes possible to establish the frequency equation of the stay cable,

$$\begin{gathered} \left(\frac{\mathrm{E}Im}{S^2}\eta^2 - 1\right)^2 \left\{ \begin{array}{l} cot\left[\left(1 - \frac{l_1}{L} - \frac{l_2}{L}\right)L\sqrt{\frac{m}{S}}\eta\right]cot\left[\frac{l_2}{L}L\sqrt{\frac{m}{S}}\eta\right] + cot\left(\frac{l_1}{L}L\sqrt{\frac{m}{S}}\eta\right)cot\left[\frac{l_2}{L}L\sqrt{\frac{m}{S}}\eta\right] \\ +cot\left(\frac{l_1}{L}L\sqrt{\frac{m}{S}}\eta\right)cot\left[\left(1 - \frac{l_1}{L} - \frac{l_2}{L}\right)L\sqrt{\frac{m}{S}}\eta\right] - 1 \end{array} \right\} \\ -\left(\frac{\mathrm{E}Im}{S^2}\eta^2 - 1\right) \left\{ \begin{array}{l} \langle cot\left[\left(1 - \frac{l_1}{L} - \frac{l_2}{L}\right)L\sqrt{\frac{m}{S}}\eta\right] + cot\left[\frac{l_2}{L}L\sqrt{\frac{m}{S}}\eta\right]\rangle \frac{c_{eq}}{\sqrt{mS}}i \\ +\langle cot\left[\left(1 - \frac{l_1}{L} - \frac{l_2}{L}\right)L\sqrt{\frac{m}{S}}\eta\right] + cot\left(\frac{l_1}{L}L\sqrt{\frac{m}{S}}\eta\right)\rangle \frac{K_D(1+i\lambda)}{\eta\sqrt{mS}} \end{array} \right\} \\ = -\frac{C_{eq}}{\sqrt{mS}}\frac{K_D}{\sqrt{mS}}\frac{i(1+i\lambda)}{\eta}. \end{gathered} \tag{6}$$

Let h_j be the complex eigenvalue corresponding to the j^{th} oscillation mode,

$$h_j = \sigma_j + i\phi_j = \frac{\eta_j}{\omega_1^0}\left(-\xi_j + i\sqrt{1-\xi_j^2}\right), \tag{7}$$

$$\sigma_j = Re\left(h_j\right) = \frac{\eta_j}{\omega_1^0}\left(-\xi_j\right); \phi_j = Im(h_j) = \frac{\eta_j}{\omega_1^0}\sqrt{1-\xi_j^2}, \tag{8}$$

$$\phi_j = Im(h_j) = \frac{\eta_j}{\omega_1^0}\sqrt{1-\xi_j^2}, \tag{9}$$

$$\xi_j = \sqrt{1 + \frac{\phi_j^2}{\sigma_j^2}}, \tag{10}$$

where ω_1^0 represents the fundamental oscillation frequency of the stay cable, ξ_j denotes the damping ratio of the stay cable in the j^{th} oscillation mode.

Substituting Eqs. (7, 8, 9 and 10) into Eq. (6) and expanding after separating the real and imaginary parts, the system of Eqs. (11) and (12) is obtained, for the real part,

$$\begin{aligned}
&[(A-1)^2-4B^2]\left[\begin{array}{c}\frac{sin\ 2asin2c-sinh2bsinh2d}{M_1M_2}+\frac{sin\ 2csin2e-sinh2dsinh2f}{M_2M_3}\\ +\frac{sin\ 2asin2e-sinh2bsinh2f}{M_1M_3}-4\end{array}\right]\\
&+[4B(A-1)]\left[\begin{array}{c}\frac{sin\ 2asinh2d+sinh2bsin2c}{M_1M_2}+\frac{sin2csinh2f+sinh2dsin2e}{M_2M_3}\\ +\frac{sin2asinh2f+sinh2bsin2e}{M_1M_3}\end{array}\right]\\
&+2(1-A)\left[\left(\frac{sin2a}{M_1}+\frac{sin2c}{M_2}\right)T_1+\left(\frac{sinh2b}{M_1}+\frac{sinh2d}{M_2}\right)T_2+\left(\frac{sin2a}{M_1}+\frac{sin2e}{M_3}\right)T_3+\left(\frac{sinh2b}{M_1}+\frac{sinh2f}{M_3}\right)T_4\right]\\
&+4B\left[\left(\frac{sin2a}{M_1}+\frac{sin2c}{M_2}\right)T_2-\left(\frac{sinh2b}{M_1}+\frac{sinh2d}{M_2}\right)T_1+\left(\frac{sin2a}{M_1}+\frac{sin2e}{M_3}\right)T_4-\left(\frac{sinh2b}{M_1}+\frac{sinh2f}{M_3}\right)T_3\right]\\
&+4(T_1T_3-T_2T_4)=0,
\end{aligned} \tag{11}$$

and for the imaginary part,

$$\begin{aligned}
&-\left[(A-1)^2-4B^2\right]\left[\begin{array}{c}\frac{sin\ 2asinh2d+sinh2bsin2c}{M_1M_2}+\frac{sin\ 2csinh2f+sinh2dsin2e}{M_2M_3}\\ +\frac{sin\ 2asinh2f+sinh2bsin2e}{M_1M_3}\end{array}\right]\\
&+4B[A-1]\left[\begin{array}{c}\frac{sin\ 2asin2c-sinh2bsinh2d}{M_1M_2}+\frac{sin\ 2csin2e-sinh2dsinh2f}{M_2M_3}\\ +\frac{sin\ 2asin2e-sinh2bsinh2f}{M_1M_3}-4\end{array}\right]\\
&+2[1-A]\left[\left(\frac{sin2a}{M_1}+\frac{sin2c}{M_2}\right)T_2-\left(\frac{sinh2b}{M_1}+\frac{sinh2d}{M_2}\right)T_1+\left(\frac{sin2a}{M_1}+\frac{sin2e}{M_3}\right)T_4-\left(\frac{sinh2b}{M_1}+\frac{sinh2f}{M_3}\right)T_3\right]\\
&-4B\left[\left(\frac{sin2a}{M_1}+\frac{sin2c}{M_2}\right)T_1+\left(\frac{sinh2b}{M_1}+\frac{sinh2d}{M_2}\right)T_2+\left(\frac{sin2a}{M_1}+\frac{sin2e}{M_3}\right)T_3+\left(\frac{sinh2b}{M_1}+\frac{sinh2f}{M_3}\right)T_4\right]\\
&+4[T_1T_4+T_2T_3]=0,
\end{aligned} \tag{12}$$

in which

$$A=\Delta\left(\sigma^2-\phi^2\right), B=\Delta\sigma\phi, \tag{13}$$

$$\begin{aligned}
&a=\pi\left(1-\tfrac{l_1}{L}-\tfrac{l_2}{L}\right)\sigma, b=\pi\left(1-\tfrac{l_1}{L}-\tfrac{l_2}{L}\right)\phi,\\
&c=\pi\tfrac{l_2}{L}\sigma, d=\pi\tfrac{l_2}{L}\phi, e=\pi\tfrac{l_1}{L}\sigma, f=\pi\tfrac{l_1}{L}\phi,
\end{aligned} \tag{14}$$

$$\begin{aligned}
&M_1=cosh^2b-cos^2a=cosh^2\left[\pi\left(1-\tfrac{l_1}{L}-\tfrac{l_2}{L}\right)\phi\right]-cos^2\left[\pi\left(1-\tfrac{l_1}{L}-\tfrac{l_2}{L}\right)\sigma\right],\\
&M_2=cosh^2d-cos^2c=cosh^2\left[\pi\tfrac{l_2}{L}\varphi\right]-cos^2\left[\pi\tfrac{l_2}{L})\sigma\right]\\
&M_3=cosh^2f-cos^2e=cosh^2\left[\pi\tfrac{l_1}{L}\phi\right]-cos^2\left[\pi\tfrac{l_1}{L}\sigma\right],
\end{aligned} \tag{15}$$

$$\begin{aligned}
&T_1=\Theta\frac{\frac{\Theta}{\Phi_S}\sigma}{\left(\frac{\Theta}{\Phi_S}\sigma\right)^2+\left(1-\frac{\Theta}{\Phi_S}\phi\right)^2}, T_2=\Theta\frac{\left(1-\frac{\Theta}{\Phi_S}\phi\right)}{\left(\frac{\Theta}{\Phi_S}\sigma\right)^2+\left(1-\frac{\Theta}{\Phi_S}\phi\right)^2}\\
&T_3=\Phi_D\frac{\sigma+\lambda\phi}{\sigma^2+\phi^2}, T_4=\Phi_D\frac{\lambda\sigma-\phi}{\sigma^2+\phi^2},
\end{aligned} \tag{16}$$

$$\Delta = \pi^2 \frac{EJ}{SL^2}, \Theta = \frac{C}{\sqrt{mS}}, \tag{17}$$

$$\Phi_S = \frac{K_S L}{\pi S}, \Phi_D = \frac{K_D L}{\pi S}. \tag{18}$$

The parameter Δ encompasses the unique characteristics of the initial data related to the stay cable, whereas Θ and Φ_S respectively represent the fundamental properties of the viscous damper and the viscous damper support stiffness. Additionally, Φ_D accounts for the fundamental properties of the HDR damper. In accordance with the initial specifications governing the stay cable, the viscous damper, and the HDR damper, the solution to Eqs. (11) and (12) is utilized to ascertain the values of σ and φ. Subsequently, these σ and φ values are employed to determine the damping ratio ξ_j for the j^{th} mode of oscillation in the stay cable using Eq. (10).

Equations (11) and (12) depict a complex nonlinear equation system with two crucial variables: σ and Φ. In Fig. 2, an intricate iterative algorithm is presented, carefully crafted to address the challenges of solving this system. Its primary objective is to determine the damping ratio of the stay cable, considering both a viscous damper and an HDR damper. Furthermore, this algorithm considers the nuances in the viscous damper support stiffness and the intrinsic bending stiffness factor EJ of the stay cable. To embark on this computational journey, the process is initiated by inputting the initial parameters governing the stay cable, the viscous damper, the viscous damper support stiffness, and the HDR damper. With this foundational work in place, a structured iterative approach is employed to tackle the nonlinear system of Eqs. (11) and (12), persisting until convergence criteria are met. What emerges from this intricate process is a wealth of valuable insights. For each distinct set of initial parameters, $\Delta, \Theta, \Phi_S, \Phi_D, \lambda, l_1/L$, and l_2/L, critical information is extracted. Specifically, the damping ratio ξ_j can be determined, shedding light on the energy dissipation characteristics of the stay cable. Additionally, the oscillation frequency η_j can be pinpointed, providing insights into the inherent vibrational behavior of the stay cable within its j^{th} mode of oscillation.

2.2 Verification of analytical model

To verify the analytical outcomes derived from the model, comparative analyses with prior study results are performed as outlined below:

Case 1: A stay cable fitted exclusively with a viscous damper

In this case, the study results are juxtaposed with those of Fujino and Hoang (2008). In detail, the initial parameters related to the HDR damper in the author's computational model are assumed to be zero ($K_D = 0, \lambda = 0, l_2 = 0$). To ensure consistency, the stiffness parameter for the viscous damper is adjusted to align with the values used as $K = \pi C l_1/(L(mS)^{0.5})$. Consequently, Eqs. (11) and (12) are reformulated, for the real part,

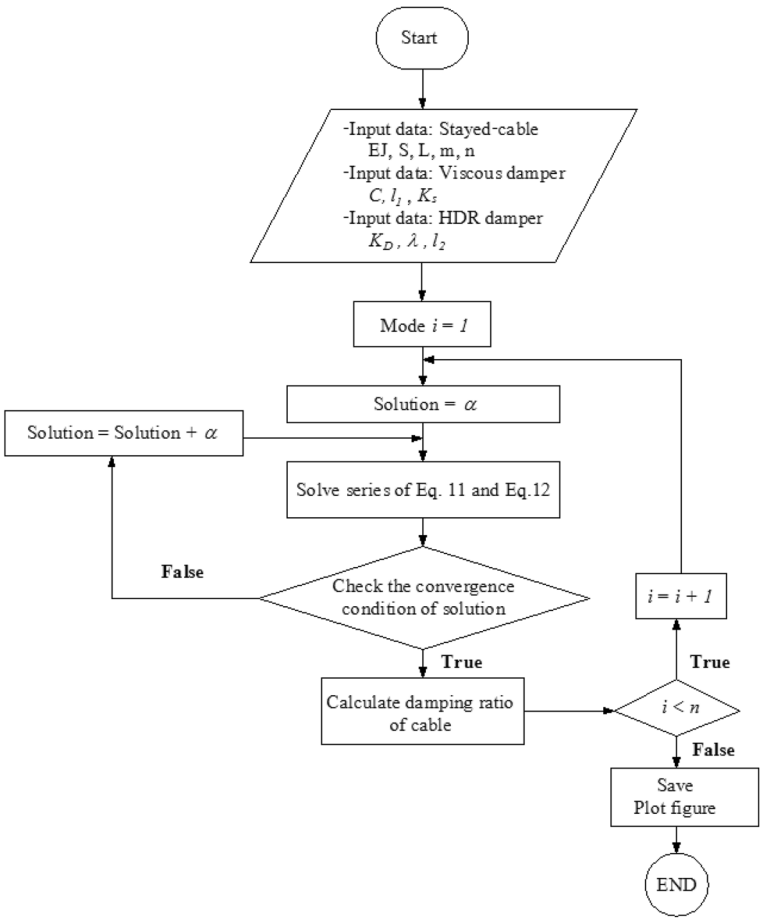

Fig. 2 Algorithm flowchart for solving nonlinear equations to determine the damping ratio of a stay cable equipped with a combination of viscous and HDR dampers

$$\begin{aligned}&\left[\Delta\left(\sigma^2-\phi^2\right)-1\right]\left[\frac{sin[2\pi(1-\frac{l_1}{L})\sigma]}{M_1}+\frac{sin(2\pi\frac{l_1}{L}\sigma)}{M_2}\right]\Phi_S\\&+2\Delta\sigma\phi\left(\frac{sinh[2\pi(1-\frac{l_1}{L})\phi]}{M_1}+\frac{sin(2\pi\frac{l_1}{L}\phi)}{M_2}\right)-2\Theta\frac{\frac{\Theta}{\Phi_S}\sigma}{\left(\frac{\Theta}{\Phi_S}\sigma\right)^2+\left(1-\frac{\Theta}{\Phi_S}\phi\right)^2}=0\end{aligned},\tag{19}$$

and for the imaginary part,

$$\begin{aligned}&\left[1-\Delta\left(\sigma^2-\phi^2\right)\right]\left[\frac{sinh[2\pi(1-\frac{l_1}{L})\phi]}{M_1}+\frac{sin(2\pi\frac{l_1}{L}\phi)}{M_2}\right]\\&+2\Delta\sigma\phi\left[\frac{sin[2\pi(1-\frac{l_1}{L})\sigma]}{M_1}+\frac{sin(2\pi\frac{l_1}{L}\sigma)}{M_2}\right]-2\Theta\frac{\left(1-\frac{\Theta}{\Phi_S}\phi\right)}{\left(\frac{\Theta}{\Phi_S}\sigma\right)^2+\left(1-\frac{\Theta}{\Phi_S}\phi\right)^2}=0\end{aligned}.\tag{20}$$

The iterative procedure, showcased in Fig. 2, is utilized to resolve Eqs. (19) and (20), aiming to ascertain the damping ratio of the stay cable when incorporating a viscous damper. The study outcomes acquired by the author's team are subsequently juxtaposed with those documented in a prior investigation (Fujino and Hoang 2008), as visually presented in Fig. 3.

The results presented in Fig. 3 unveil an intriguing correlation. When exclusively examining scenarios involving a stay cable equipped with an appended viscous damper, with meticulous consideration of factors such as bending stiffness EJ and the viscous damper support stiffness K_S, the study's outcomes harmoniously align with the groundbreaking work conducted by Fujino and Hoang (2008). This alignment of results not only supports the credibility of the investigation but also underscores the robustness and consistency of the experimental approach.

Case 2: A stay cable equipped solely with an HDR damper

In this case, the results from a stay cable model with an HDR damper are calculated and compared with those presented by Fujino and Hoang (2008) and Cu and Han (2015). In this case, the initial parameters related to the viscous damper in the author's model are set to zero ($C = 0, l_1 = 0$). To align with the input parameters specified in Fujino and Hoang (2008) and Cu and Han (2015), the stiffness parameter of the HDR damper is redefined as $K = l_2 K_D / S$. Consequently, Eqs. (11) and (12) undergo a reformulation, for the real part,

$$\left[\frac{sin[2\pi(1-\frac{l_2}{L})\sigma]}{M_1} + \frac{sin(2\pi\frac{l_2}{L}\sigma)}{M_2}\right] + 2\Phi_D \frac{\sigma + \lambda\phi}{\sigma^2 + \phi^2} = 0, \tag{21}$$

and for the imaginary part,

$$\left[\frac{sinh[2\pi(1-\frac{l_2}{L})\phi]}{M_1} + \frac{sin(2\pi\frac{l_2}{L}\phi)}{M_2}\right] + 2\Phi_D \frac{\phi - \lambda\sigma}{\sigma^2 + \phi^2} = 0. \tag{22}$$

By applying the iterative algorithm illustrated in Fig. 2, the solutions can be obtained by solving the system of Eqs. (21) and (22). This computational approach is instrumental in obtaining a precise cable damping ratio, especially when an HDR damper is attached

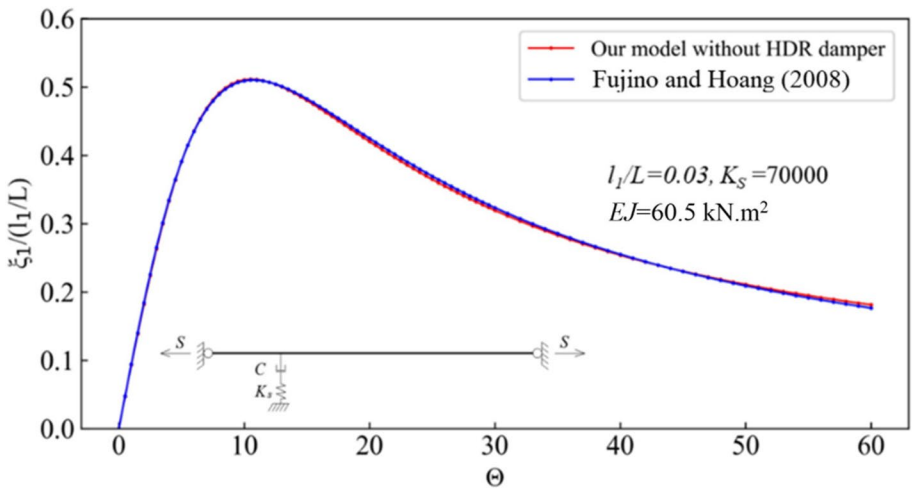

Fig. 3 Comparison of results for the case with a viscous damper attached

to the stay cable. The analytical results provide a comprehensive insight into the stay cable's first damping ratio in this specific configuration. Notably, these results align remarkably well with the previously published study outcomes detailed in Fujino and Hoang (2008) and Cu and Han (2015). Figure 4 serves as a visual testament to the congruence between the present study and the established body of knowledge.

In this case, a rigorous comparative analysis is conducted with those detailed by Hoang and Fujino (2008). It is of utmost importance to acknowledge that the stay cable model elucidated in Hoang and Fujino (2008) regrettably disregards the pivotal influences of the intrinsic bending stiffness EJ inherent to the stay cable and the inherent damper support stiffness. In response to this critical oversight, the initial parameters within the model are fine-tuned, aligning them with the conditions elucidated in the work of Hoang and Fujino (2008). Specifically, EJ is set zero and two distinct scenarios for the stiffness parameter K_S, one of which is $K_S = \infty$ and the other, 6000 kN/m, are examined in strict accordance with the precise input parameters specified in their investigation. This leads to recalibrate Eqs. (11) and (12), thereby offering a nuanced reflection of the precise conditions under scrutiny, and culminating in the formulation of the following expressions, for the real part,

$$\begin{aligned}&\left[\frac{\sin 2a\sin 2c-\sinh 2b\sinh 2d}{M_1M_2}+\frac{\sin 2c\sin 2e-\sinh 2d\sinh 2f}{M_2M_3}+\frac{\sin 2a\sin 2e-\sinh 2b\sinh 2f}{M_1M_3}-4\right]\\&+2\left[\left(\frac{\sinh 2b}{M_1}+\frac{\sinh 2d}{M_2}\right)\Theta+\left(\frac{\sin 2a}{M_1}+\frac{\sin 2e}{M_3}\right)T_3+\left(\frac{\sinh 2b}{M_1}+\frac{\sinh 2f}{M_3}\right)T_4\right]-4\Theta T_4=0,\end{aligned} \tag{23}$$

and for the imaginary part,

$$\begin{aligned}&-\left[\frac{\sin 2a\sinh 2d+\sinh 2b\sin 2c}{M_1M_2}+\frac{\sin 2c\sinh 2f+\sinh 2d\sin 2e}{M_2M_3}+\frac{\sin 2a\sinh 2f+\sinh 2b\sin 2e}{M_1M_3}\right]\\&+2\left[\left(\frac{\sin 2a}{M_1}+\frac{\sin 2c}{M_2}\right)\Theta+\left(\frac{\sin 2a}{M_1}+\frac{\sin 2e}{M_3}\right)T_4-\left(\frac{\sinh 2b}{M_1}+\frac{\sinh 2f}{M_3}\right)T_3\right]+4[\Theta T_3]=0\end{aligned}. \tag{24}$$

Directing the attention to the application of the iterative algorithm presented in Fig. 2, a computational journey to grapple with the complex system of Eqs. (23) and

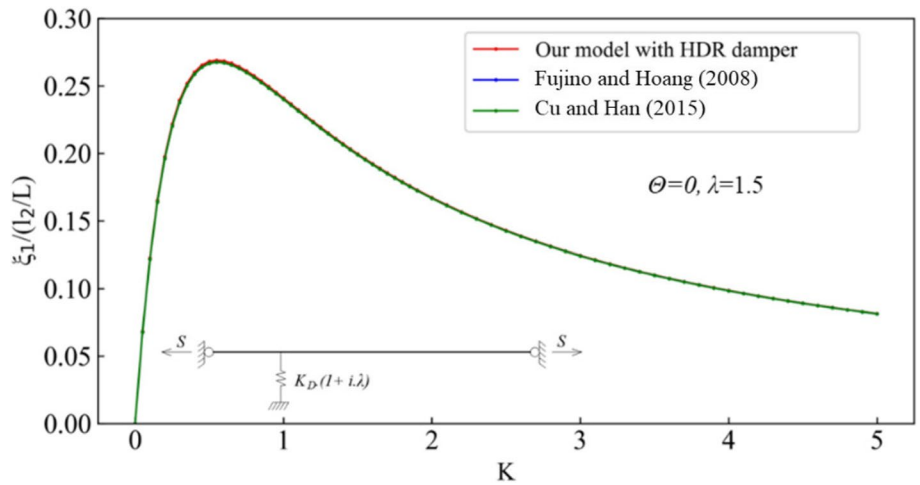

Fig. 4 Comparison of results for the case with an HDR damper attached

(24) is embarked on. This endeavor is dedicated to unveiling the mysteries of the damping ratio in stay cables, particularly when they are equipped with both a viscous damper and an HDR damper. It's important to note that this path without considering the inherent damper support stiffness ($K_S = \infty$) and the inherent bending stiffness of the stay cable ($EJ = 0$) is traversed. The finding in Fig. 5 shows that the analysis regarding the damping ratio of the stay cable, curated by the author, exhibits a remarkable agreement with the results chronicled in Hoang and Fujino (2008), especially when $K_S = \infty$. However, the narrative takes an intriguing turn when K_S is set to 6000 kN/m. Here, a noticeable decline in the damping ratio of the stay cable becomes evident, as depicted by the trends in Fig. 5. This revelation underscores the pivotal role played by the viscous damper support stiffness in shaping the operational effectiveness of the damper. Furthermore, it emphasizes the substantial impact of this stiffness parameter in significantly reducing the maximum attainable damping ratio for the stay cable.

The analytical results concerning the first damping ratio of the stay cable, as derived by the author across all three rigorously validated models, exhibit a commendable alignment with previously documented study results (Fujino and Hoang 2008; Cu and Han 2015). This synchronization reaffirms the credibility and robustness of the oscillation analysis model proposed by the author. Notably, this model comprehensively considers critical factors, such as the viscous damper support stiffness and the bending stiffness intrinsic to the stay cable. As proceed, this comprehensive model will serve as an invaluable tool for delving into the ramifications of parameters associated with both the viscous damper and the HDR damper. These investigations will shed light on how these parameters influence the maximum attainable damping ratio of the stay cable, providing crucial insights into the optimization of damping systems in subsequent sections.

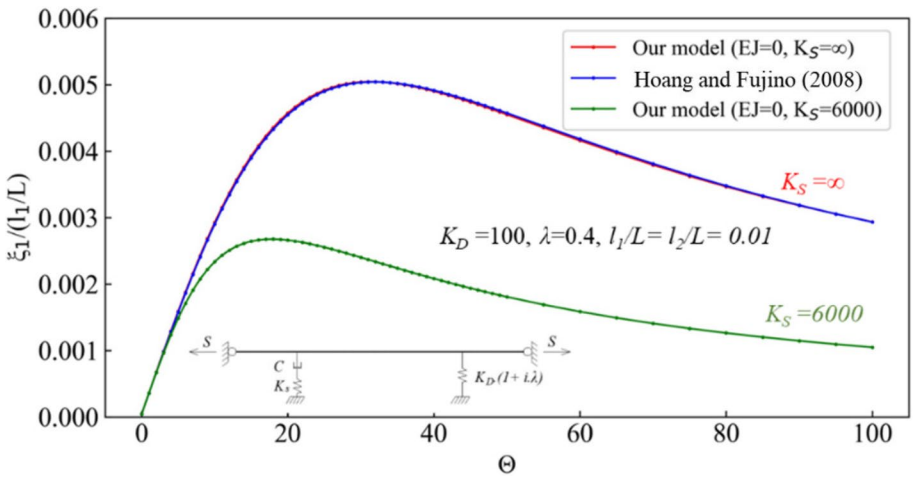

Fig. 5 Comparison of results for the case with a viscous damper and an HDR damper attached

3 Results and discussions

3.1 Influence of the viscosity coefficient *C* of the viscous damper on the first damping ratio of the stay cable

The viscosity coefficient C of the viscous damper is denoted by the parameter $\Theta = C/(mS)^{0.5}$. To delve deeper into the subject, an exploration of the variation in the first damping ratio ξ_1 of the stay cable across the entire spectrum of Θ values is embarked on, ranging from 0 to 100. These values correspond to a diverse set of initial conditions, encompassing the installation position of the damper, $l_i/L = (0.01, 0.02, 0.03, 0.04, 0.05)$, the spring factor of the HDR damper, $K_D = 1150$kN/m, the loss coefficient of the HDR damper $\lambda = 0.4$ and the viscous damper support stiffness $K_S = 2000$kN/m. The results of this investigation are vividly depicted in the graphical representation presented in Fig. 6. This examination of how Θ influences ξ_1 provides an intricate perspective on the interplay among these various parameters.

The results gleaned from the analysis unveil a consistent pattern: for each set of initial parameters, including l_i/L, K_D, K_S, and λ, the first damping ratio ξ_1 of the stay cable steadily increases with the escalation of Θ. However, once ξ_1 reaches its zenith value, denoted as ξ_{1max}, any further increase in Θ prompts a gradual decline in ξ_1. Consequently, at the point where the first damping ratio peaks ξ_{1max}, the optimal parameter Θ_{opt} can be pinpointed. Subsequently, the optimal viscosity coefficient for the viscous damper C_{opt} can deduced through the equation $\Theta_{opt} = C_{opt}/(mS)^{0.5}$.

As the ratio l_i/L increases, signifying the damper's placement closer to the midpoint of the stay cable, the damping ratio of the cable experiences a commensurate increase, indicative of the damper's enhanced effectiveness. However, considerations of aesthetics and the ease of device manufacturing and maintenance frequently dictate the selection of damper placement within the range of 2–5% of the cable's length. With distinct positions represented by varying l_i/L values, the maximum attainable damping ratio for the stay cable naturally varies as well. Consequently, in the design of stay cable damping systems employing viscous dampers, it is customary to preselect the damper's location for the sake of convenience in device manufacturing and maintenance. Subsequently, a

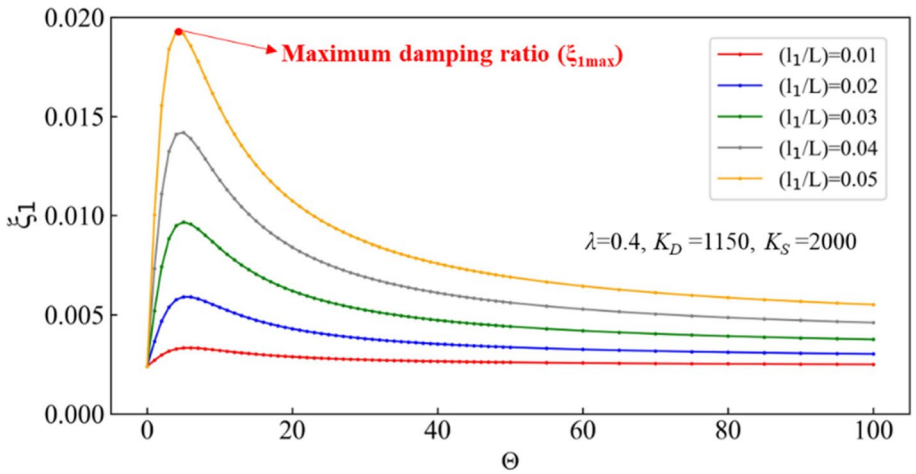

Fig. 6 The relationship between the fundamental properties of the viscous damper Θ and the first damping ratio ξ_1 of the stay cable

thorough evaluation and computation of the optimal viscosity coefficient for the viscous damper are conducted to optimize vibration reduction efficiency for the stay cable.

3.2 Influence of the viscous damper support stiffness on the first damping ratio of the stay cable

The stiffness of viscous damper support K_S plays a crucial role in the dynamics of stay cables. This stiffness is quantified by the fundamental parameter Φ_S, calculated as $\Phi s = K_S L/(\pi S)$, where L represents the length of the cable and S is the tension force of the stay cable. In this section, a comprehensive investigation is delved into, exploring how variations in Φ_S impact the first damping ratio ξ_1 of the stay cable. The exploration covers a wide spectrum of Φ_S values, ranging from 5 to 100, reflecting diverse scenarios. A set of initial parameters is considered given as the installation positions of the damper l_1/L selected from the range (0.01, 0.02, 0.03, 0.04, 0.05), the location of the HDR damper l_2/L fixed at 0.03, and additional parameters such as the loss coefficient of the HDR damper ($\lambda = 0.4$) and the spring factor of the HDR damper ($K_D = 1150kN/m$) remained constant.

The results shown in Fig. 7 reveal the significant impact of the viscous damper support stiffness K_S, on the achievable first damping ratio ξ_1 of the stay cable. As K_S diminishes, the damping ratio of the cable experiences a sharp decline. This pattern underscores the high sensitivity of stay cable damping systems to variations in the viscous damper support stiffness. In practical stay cable damping design, it is often convenient to assume that the viscous damper support's stiffness is infinitely rigid ($K_S = \infty$). However, this assumption can lead to substantial disparities between the actual measured damping ratio and the theoretically predicted values. Within the examined range of Φ_S from 5 to 100, notable reductions in the damping ratio are observed as the damper attachment position along the stay cable l_1/L is shifted from 0.01 to 0.05. These reductions are quantified as follows: 46.26%, 62.36%, 62.93%, 58.73%, and 52.42%, respectively. Such substantial variations underscore the pivotal role played by the viscous damper support stiffness in the precise calculation and prediction of the maximum attainable damping ratio for the stay cable.

3.3 Influence of the spring factor of the HDR damper on the first damping ratio of the stay cable

The spring factor of the HDR damper K_D plays a pivotal role in the dynamics of a stay cable system. It's characterized by the parameter Φ_D, which is defined as $\Phi_D = K_D L/(\pi S)$. To investigate the relationship between the HDR damper's stiffness and the first damping ratio ξ_1 of the stay cable, a wide range of Φ_D values, ranging from 0 to 10, with several initial conditions are considered. These initial conditions are carefully selected to represent real-world scenarios. Damper attachment positions l_1/L and l_2/L, both equal to 0.03, reflecting typical installation practices are examined. The loss coefficient of the HDR damper λ is varied from 0.4 to 2.0 to account for different material properties. Additionally, the viscous damper support stiffness K_S is kept constant in 2000 kN/m, a value commonly encountered in practice.

The results shown in Fig. 8 provide an understanding of how the spring factor of the HDR damper impacts the first damping ratio ξ_1 of the stay cable. Initially, ξ_1 increases

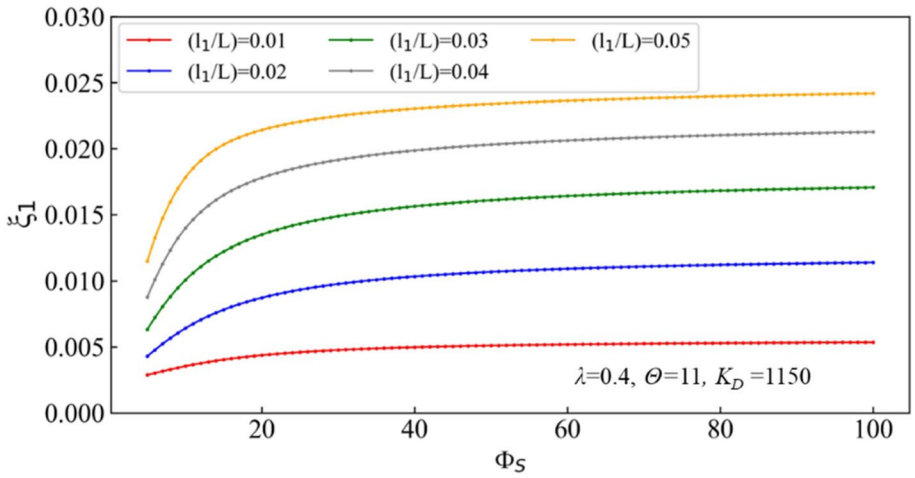

Fig. 7 The relationship between the fundamental properties of the viscous damper support stiffness Φ_S and the first damping ratio ξ_1 of the stay cable

with the increase of Φ_D, reflecting the enhanced damping capacity of the HDR damper. However, a fascinating twist occurs when ξ_1 reaches its zenith, denoted as ξ_{1max}. Beyond this point, as Φ_D continues to rise, ξ_1 begins to decline. This decline highlights the intricate interplay between the HDR damper's stiffness and the cable's damping characteristics. The significance of these results extends to practical applications in the field of cable damping design. Engineers and designers often face the challenge of optimizing damper devices to achieve the desired damping performance. At the ξ_{1max} point, where the maximum damping ratio is attained, the optimal value of Φ_D, denoted as Φ_{Dopt}, is pinpointed. This value unlocks the optimal stiffness K_{Dopt} of the HDR damper device through the relationship $\Phi_{Dopt} = K_{Dopt}L/(\pi S)$. In essence, it provides a precise blueprint for designing dampers that offer optimal vibration reduction efficiency for stay cables. Furthermore, the investigation underscores the sensitivity of the optimal HDR damper stiffness to variations in the loss coefficient λ of the HDR damper material. Different material properties necessitate distinct values of K_{Dopt}. This nuanced understanding paves the way for tailored solutions, ensuring that cable damping systems are finely tuned to their specific operational requirements.

3.4 Influence of the loss coefficient of the HDR damper on the first damping ratio of the stay cable

The relationship between the first damping ratio ξ_1 of stay cables and the loss coefficient λ of the HDR damper is also examined. The investigation is carried out by varying λ, within the range (0–20), influencing to ξ_1, while maintaining specific initial conditions. These conditions included fixed damper attachment positions, l_1/L, and l_2/L, set at 0.03, and a consistent Θ value of 11. The viscous damper support stiffness K_S remained unwavering in 2000 kN/m.

Figure 9 illuminates the intricate relationship between the loss coefficient λ of the HDR damper and the damping ratio ξ_1 of the stay cable. Initially, as λ increases, ξ_1 experiences a harmonious ascent, indicating the HDR damper's enhanced damping performance, culminating at ξ_{1max}. However, beyond this critical threshold, ξ_1

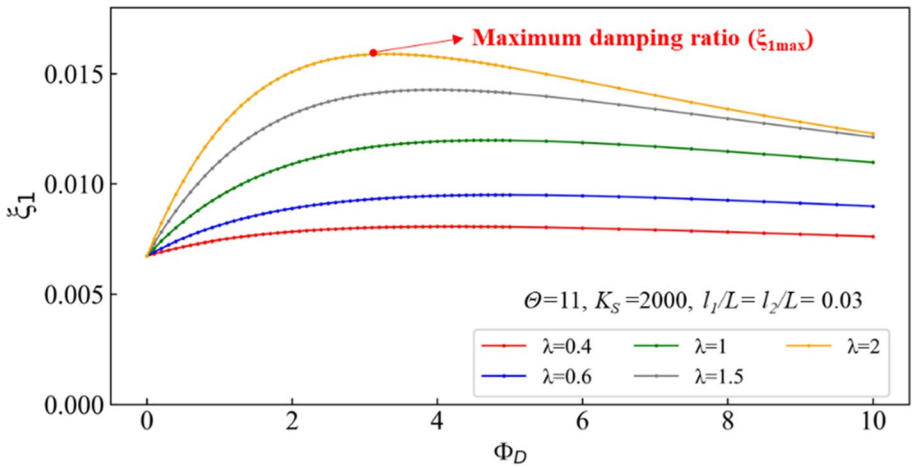

Fig. 8 The relationship between the fundamental properties of the HDR damper Φ_D and the first damping ratio ξ_1 of the stay cable

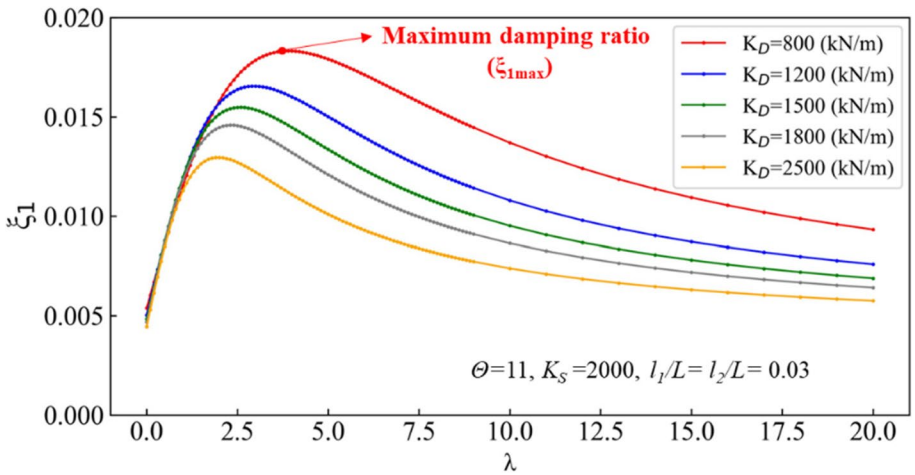

Fig. 9 The relationship between the loss coefficient of the HDR damper λ and the damping ratio ξ_i of the stay cable

gracefully diminishes with each incremental λ increment. When the juncture of ξ_{1max} is reached, the optimal λ value, denoted as λ_{opt}, can be precisely determined. This pivotal value is instrumental in achieving maximum efficiency in mitigating cable vibrations, considering aesthetic aspects, ease of installation, and maintenance. Furthermore, the investigation underscores the sensitivity of the optimal stiffness of the HDR damper K_D. Distinct K_D values correspond to specific λ_{opt} values. Therefore, when designing cable damping systems employing HDR dampers, it is prudent to preselect damper attachment positions, considering aesthetics, practical installation, and maintenance convenience. Subsequently, an analysis can be conducted to ascertain the optimal values for both K_D and λ, ensuring the highest level of efficiency in reducing cable vibrations.

3.5 Influence of the stay cable's bending stiffness on the first damping ratio of the stay cable

The damping ratio of a stay cable isn't solely contingent on the characteristics of attached dampers like viscous or HDR ones. They also hinge on intrinsic cable attributes such as length L and tension S. For extended cables, a common practice involves reinforcing them by applying epoxy resin coatings, significantly enhancing their bending stiffness EJ. This augmented stiffness is quantified through a dimensionless parameter, $\Delta = \pi^2 EJ/(SL^2)$.

The investigation is further carried out to unveil how the initial damping ratio ξ_1 of the stay cable responds to variations in the Δ parameter, spanning the range (0-0.25). The results, presented in Fig. 10, illuminate a striking revelation: within this parameter spectrum, the first damping ratio of the stay cable can surge by up to 12%. This substantial amplification bears immense significance and warrants consideration when delving into the cable's oscillation analysis. Note that the survey results assume neglecting the rotational stiffness at both ends of the stay cable, and align entirely with the increase of factor R_h (Le et al. 2020).

3.6 Influence of combining two viscous and HDR dampers on the first damping ratio of the stay cable

In this section, the combined influence of two distinct dampers, namely the viscous damper and the HDR damper, on the damping ratio of a stay cable is examined. The objective is to understand how variations in the parameters of the HDR damper, specifically its stiffness K_D and the loss coefficient λ of the HDR damper, affect the optimal setting of the viscous damper, represented by the parameter Θ_{opt}.

As illustrated in Fig. 11, a notable increase in the peak value of the first damping ratio ξ_1 for the stay cable is observed. This suggests that adjusting the spring factor of the HDR damper can significantly enhance the cable's damping ratio. However, the

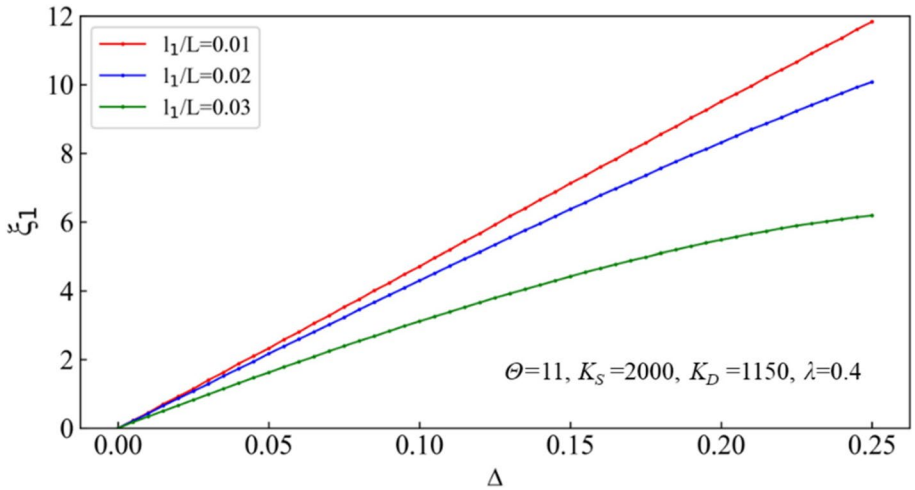

Fig. 10 The relationship between the stay cable's bending stiffness through a dimensionless parameter Δ and the first damping ratio ξ_1 of the stay cable

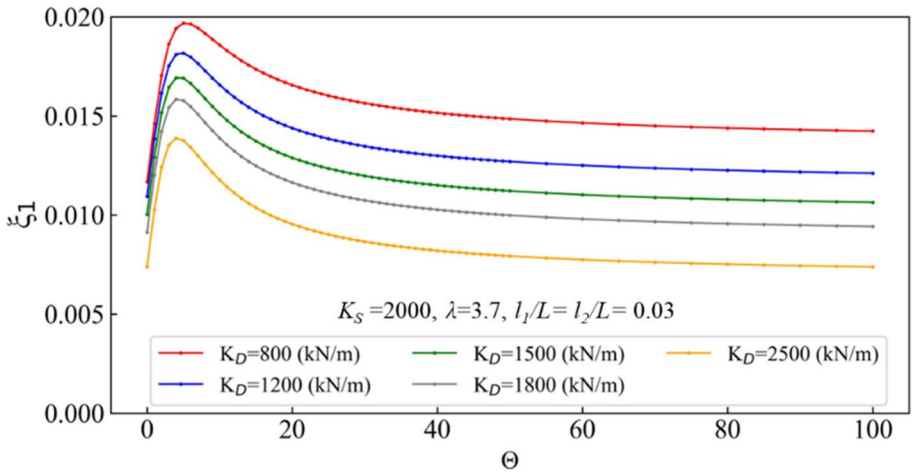

Fig. 11 The relationship between the fundamental properties of the viscous damper Θ and the first damping ratio ξ_1 of the stay cable across various K_D values

Table 1 The first damping ratioξ_{1max}variations with different HDR damper stiffness$K_D$values

K_DkN/m	800	1200	1500	1800	2500
ξ_{1max}	0.0197	0.0182	0.0169	0.0158	0.0139
Θ_{opt}	5				

optimal setting for the viscous damper denoted as Θ_{opt}, remained remarkably consistent across these variations, as depicted in Table 1.

In Fig. 12, the impact of altering the loss coefficient λ of the HDR damper within the HDR damper is explored. Once again, an increase in the peak value of ξ_1 is witnessed, signifying an improved damping ratio. Mirroring the previous scenario, the optimal parameter Θ_{opt} for the viscous damper remained nearly unaltered, as evidenced in Table 2.

The results imply that the parameters governing the behavior of the rubber damper, such as its stiffness K_D and loss coefficient λ, operate relatively independently of the optimal settings for the viscous damper. In essence, the efficacy of these two distinct dampers doesn't significantly influence one another. Instead, the combined damping effectiveness of both dampers can be approximated by summing their damping contributions.

3.7 Damping efficiency of viscous and HDR dampers on various vibrational modes of stay cable

In practical scenarios, stay cables can exhibit diverse modes of oscillation, each possessing unique characteristics. To comprehensively assess the damping efficacy of a combination of both viscous and HDR dampers across these distinct vibrational modes (n =1, 2, and 3), a detailed investigation is conducted. The damper attachment positions are uniformly set at $l_1/L = l_2/L = 0.03$, with the viscous damper support stiffness K_S at a constant of 2000 kN/m and the parameters of the HDR damper, including $K_D = 1150$kN/m and $\lambda = 0.4$.

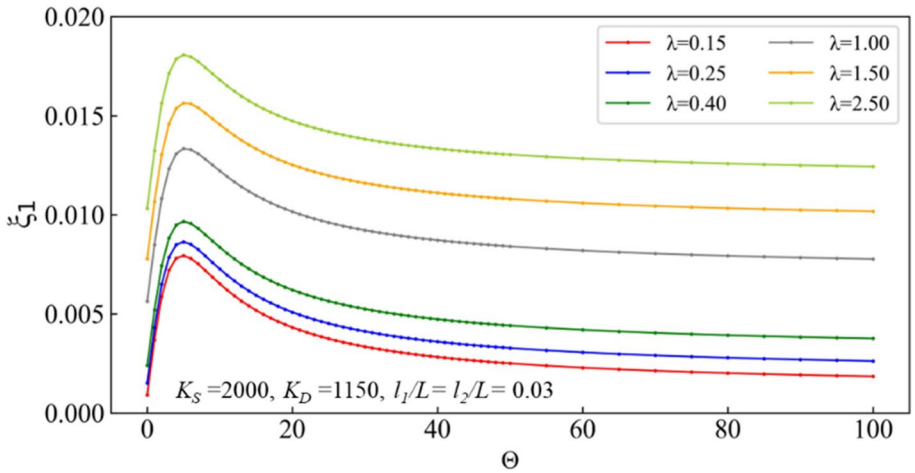

Fig. 12 The relationship between the fundamental properties of the viscous damper Θ and the first damping ratio ξ_1 of the stay cable across various λ values

Table 2 The first damping ratio ξ_{1max} variations with different loss coefficients of the HDR damper λ values

λ	0.15	0.25	0.40	1.00	1.50	2.50
ξ_{1max}	0.0079	0.0086	0.0097	0.0133	0.0156	0.0181
Θ_{opt}	5					

Figure 13 showcases the remarkable effect of the optimal viscous damper coefficient Θ_{opt1} on the first damping ratio ξ_1 in mode $n = 1$, leading to the attainment of the maximum value ξ_{1max}. However, the first damping ratio of the stay cable in modes $n = 2$ and $n = 3$ experiences a significant reduction at this specific Θ_{opt1} value. These results underscore the necessity of optimizing damper parameters tailored to the distinct vibrational modes commonly encountered in stay cables during the design phase. This approach ensures the highest degree of vibration reduction efficacy while considering practical installation, maintenance, and aesthetic factors.

3.8 *Variation in the oscillation frequency of the stay cable with damper attachments*

The natural oscillation frequency ω_1^0 of the stay cable is inherently determined by various initial parameters such as its length L, tension force S, bending stiffness EJ, and unit weight m. However, when dampers are introduced into the system, the oscillation frequency η_1 of the cable-damping system undergoes discernible alterations. Analyzing these frequency changes before and after the integration of the damper using the frequency ratio η_1/ω_1^0, as depicted in Fig. 14, reveals a noticeable rise in the system's oscillation frequency compared to the original cable configuration. Furthermore, the placement of the dampers along the cable, characterized by l_i/L, significantly influences the extent of this frequency enhancement. Nevertheless, overall, the observed increase in frequency for the suspended cable, following the attachment of the damper, remains relatively modest, not exceeding 3%.

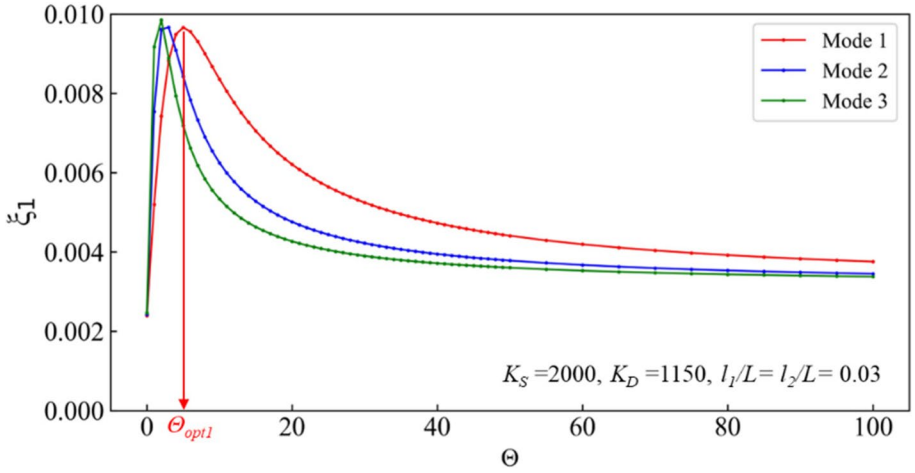

Fig. 13 The relationship between the fundamental properties of the viscous damper Θ and the first damping ratio ξ_1 of the stay cable across vibrational modes (n=1, 2, and 3)

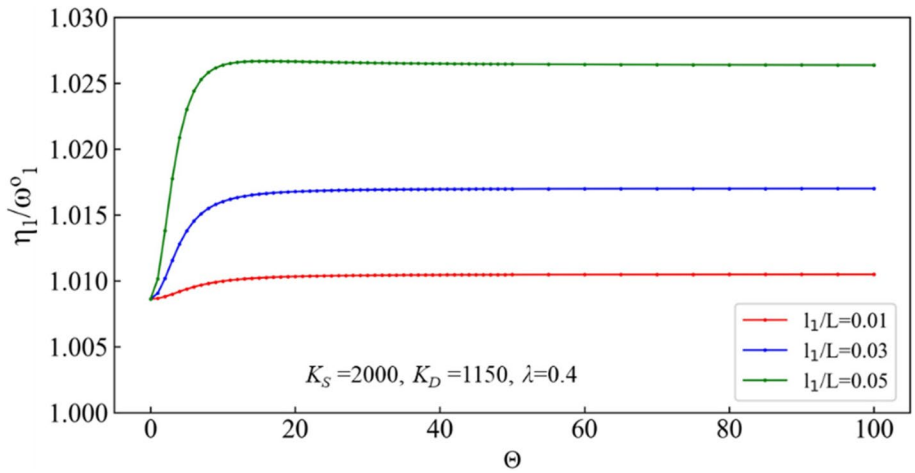

Fig. 14 The relationship between the fundamental properties of the viscous damper Θ and the oscillation frequency changes before and after the integration of the damper η_1/ω_1^0

3.9 Damping efficiency when two dampers installed on the same side of the stay cable

The damping efficiency when two dampers are installed on the same side of the stay cable is also investigated. As shown in Fig. 1, the positions of the two dampers are defined by l_1 and l_2^*. The values of l_1 and l_2^* can vary within the range of 0 to L. To consider the effect of installing two dampers on the same side of the stay cable, the fundamental damping ratio of the cable ξ_1 is investigated according to the change of parameter Θ in the range of 0 to 100, corresponding to the locations of the dampers as $l_1/L = 0.03$ and $l_2^*/L = 0.02$. The comparative results in Fig. 15 show that the damping efficiency when installing two dampers on the same side of the stay cable is much lower than in the case of installing two dampers on both sides of the stay cable. The maximum damping ratio of the stay cable when installing two dampers on the same side of the stay cable is only about 61.6% compared to the case where two dampers are installed on both sides of the stay cable. Therefore, when installing dampers, each damper should be installed on

each side of the stay cable to maximize the maximum vibration reduction effect of the stay cable.

3.10 Optimal parameters of the viscous damper and HDR damper

In practical scenarios, the damping ratio of a specific stay cable, with constant length L, unit weight m, tension force S, and bending stiffness EJ, simultaneously relies on several factors, encompassing the properties of the viscous damper (viscosity coefficient C, viscous damper support stiffness K_S and the HDR damper (stiffness K_D, loss coefficient of the HDR damper λ). When these parameters of the dampers are optimized, the cable achieves its maximum possible damping ratio. To pinpoint these optimal values, one can employ sensitivity analysis, which reveals the intricate three-dimensional interplay between the cable's first damping ratio ξ_1, the parameter Θ representing the damper's viscosity, and the damper attachment position l_1/L. Figure 16 graphically illustrates this complex relationship, offering insights into how the selection of specific damper attachment positions (determined based on factors such as aesthetics, ease of installation, and maintenance) can lead to the identification of the optimal Θ_{opt} value for the damper's viscosity coefficient.

Figure 17 unveils a three-dimensional relationship that intertwines the first damping ratio of the stay cable ξ_1 with two vital parameters Θ which reflects the viscous damper's damping efficiency, and λ signifying the loss coefficient of the HDR damper. Tailored to the precise installation location of the HDR damper denoted as l_2/L (determined by aesthetic considerations, practical installation constraints, and maintenance convenience), and the previously determined optimal value Θ_{opt} as showcased in Fig. 16; this intricate relationship guides the selection of the optimal loss coefficient λ_{opt} for the HDR damper.

Similarly, Fig. 18 unveils a trilateral relationship that parallels the preceding figures. This intricate correlation intertwines the first damping ratio of the stay cable $\xi_1$with two pivotal parameters: Φ_D symbolizing the fundamental properties of the HDR damper and λ representing the loss coefficient of the HDR damper. Contingent upon the specific mounting location of the HDR damper denoted as l_2/L (determined

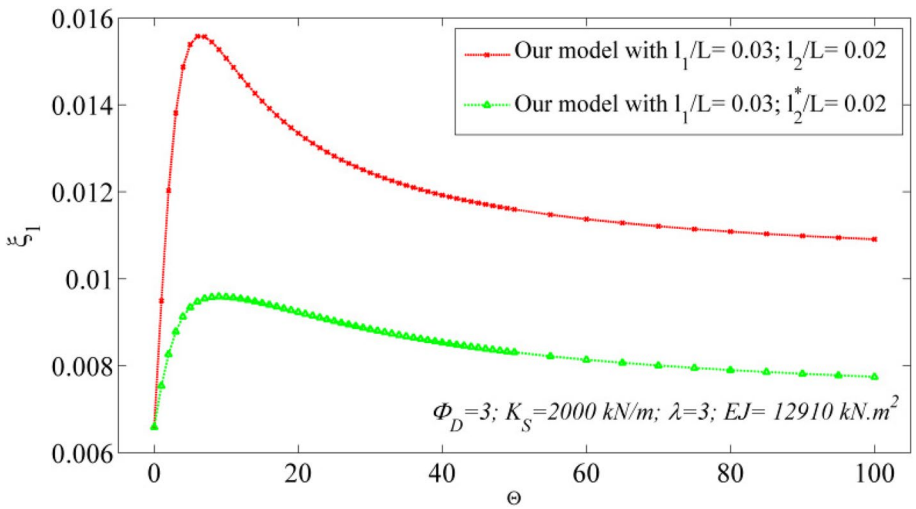

Fig. 15 Effectiveness comparison of installing two dampers on one side and both sides of the stay cable

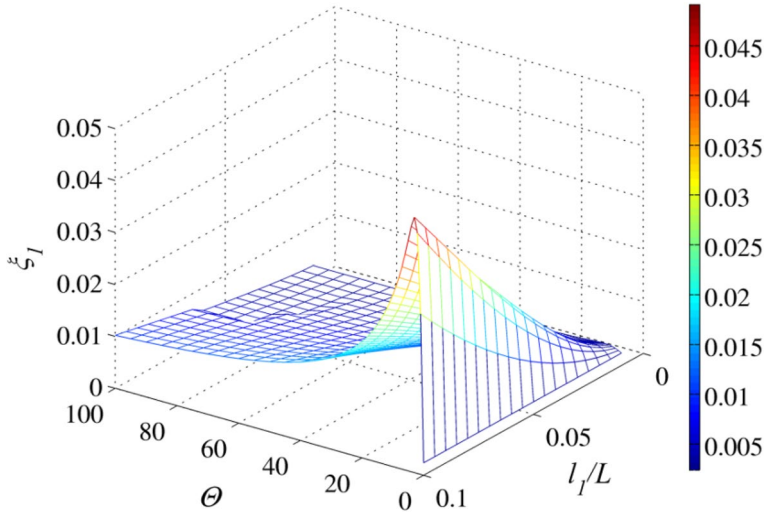

Fig. 16 The relationship between (ξ_1-Θ-l_1/L)

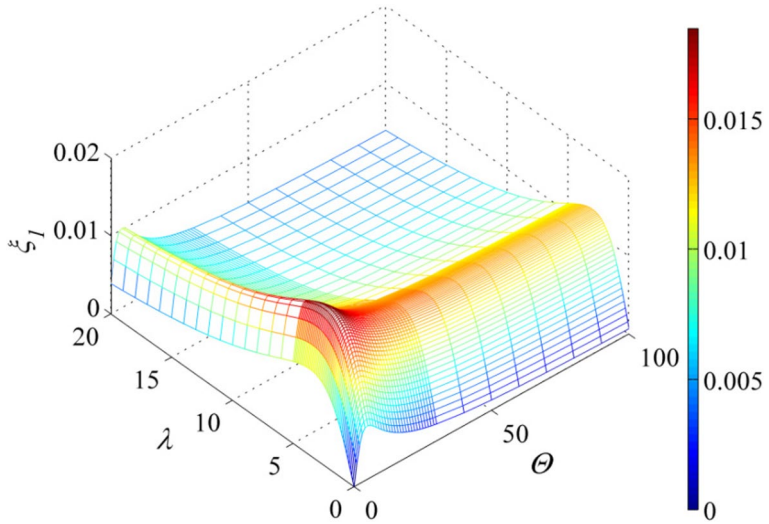

Fig. 17 The relationship between (ξ_1-Θ-λ)

through considerations of aesthetics, installation feasibility, and maintenance convenience), and informed by the previously ascertained optimal λ_{opt} value from Fig. 17, the optimal stiffness coefficient Φ_{Dopt} can be selected for the HDR damper.

As a practical example, let's consider a specific stay cable installation with dampers, precisely placed at positions $l_1/L = l_2/L = 0.03$. Utilizing the insights gained from the three-dimensional relationship between ξ_1-Θ-l_1/L (Fig. 16), the optimal parameter representing the viscosity coefficient of the viscous damper can be deduced. This optimal value, denoted as $\Phi_{opt} = 5$, is then employed as a reference point. Moving forward, the three-dimensional landscape of ξ_1-Θ-λ (illustrated in Fig. 17) is navigated through, centered around the established Φ_{opt} value of 5. Here, the optimal loss coefficient for the HDR damper, settling on $\lambda_{opt} = 3.3$, is selected.

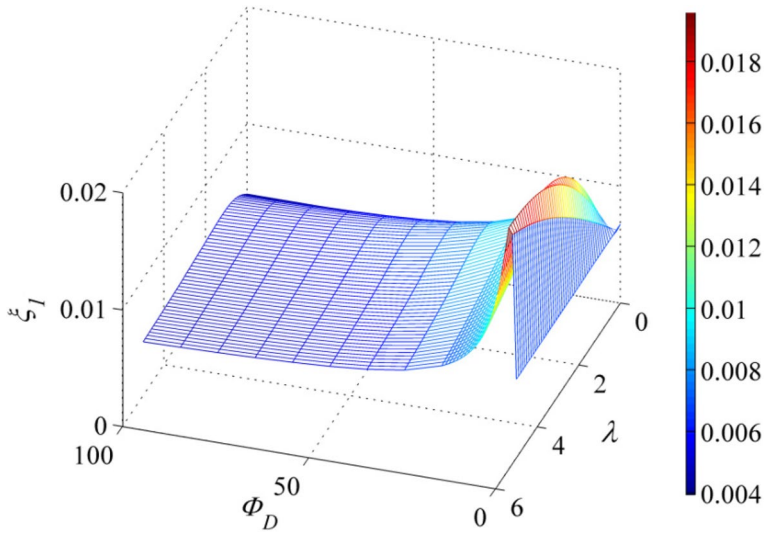

Fig. 18 The relationship between (ξ_1-Φ_D-λ)

Lastly, with the λ_{opt} value of 3.3, the three-dimensional realm of ξ_1-Φ_D-λ (Fig. 18) is delved into. In this domain, the optimal stiffness coefficient for the HDR damper is identified, landing on a value of $\Phi_D = 2$. With these precisely tuned parameters for the dampers, the pinnacle of damping efficiency for the stay cable is achieved, boasting a maximum attainable first damping ratio of $\xi_{1max} = 1.8345\%$.

Additionally, the combined impact of the viscous damper support stiffness K_S and the viscosity coefficient C of the viscous damper on the first damping ratio ξ_1 of the stay cable is explored. This intricate relationship is illustrated in a three-dimensional representation, as shown in Fig. 19. In general, it can be observed that a decrease in the viscous damper support stiffness K_S leads to a notable reduction in the effectiveness of the damper in mitigating cable vibrations. Simultaneously, variations in the viscosity coefficient C of the viscous damper also influence the first damping ratio ξ_1. Understanding the interplay between these factors is critical for precise predictions of the maximum achievable damping ratio for stay cables. It allows us to optimize the design and placement of dampers, enhancing their efficiency in reducing cable vibrations.

4 Conclusions

This study presented an oscillation model for a stay cable, introducing a novel vibration motigation approach that combines a viscous damper and an HDR damper affixed at both cable ends. This model takes into consideration not only the stay cable's bending stiffness but also the critical factors of viscous damper support flexibility. Furthermore, it goes beyond the theoretical realm by providing practical insights through rigorous validation, yielding results that align with previously established studies. From the comprehensive analysis executed within this model, several conclusions emerge:

- The proposed model excels in its capacity to furnish more precise predictions concerning the upper limits of achievable damping ratio for stay cables when

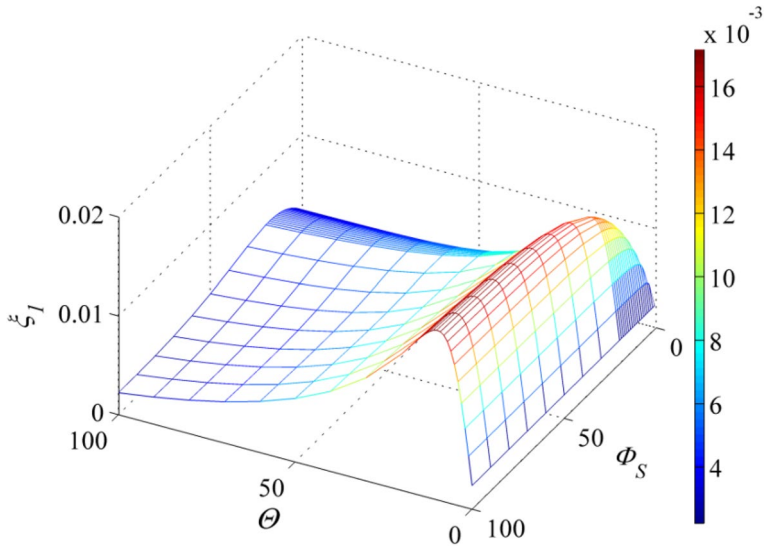

Fig. 19 The relationship between (ξ_1-Φ_S-Θ)

equipped with both viscous and HDR dampers. Its unique ability to account for viscous damper support stiffness and stay cable's bending stiffness enhances the accuracy of these forecasts.

- The result underscores that a reduction in viscous damper support stiffness substantially diminishes the cable's maximum attainable damping ratio. Conversely, when neglecting the rotational stiffness at both ends of the stay cable, an increase in the stay cable's bending stiffness significantly enhances the maximum attainable damping ratio.
- A profound insight emanates from the analysis that the vibration mitigation effect resultant from the combination of viscous and HDR dampers is an amalgamation of their vibration-reducing prowess.
- The mounting of dampers onto the stay cable modestly influences its oscillation frequency. Importantly, these changes in frequency are inversely proportional to the proximity of the damper attachment points to the stay cable's anchor locations. It is also noticed that the damping efficiency when installing two dampers on the same side of the stay cable is much lower than in the case of installing two dampers on both sides of the stay cable.
- Through a survey probing the intricate three-dimensional relationship between the cable's damping ratio and the damper parameters, this study allows for the precise identification of optimal values for viscous and HDR dampers. These values ensure the maximization of cable oscillation reduction while considering an array of critical factors, including stiffness variables and attachment locations.

In summation, this research extends the frontiers of comprehension regarding the dynamic behaviour of stay cables furnished with combined damping solutions. It not only broadens the theoretical understanding but also offers invaluable practical guidance in the design of systems that efficaciously mitigate cable vibrations, all the while accommodating the nuances of stiffness parameters and attachment locales.

Acknowledgements
The authors would like to thank the support of The University of Danang – University of Science and Technology.

Authors' contributions
DTN established the conceptualization and methodology, developed the code, performed the validation and analysis, and wrote the original draft. SQC developed the code, performed analysis and investigation. PHN performed investigations, visualized, and revised the manuscript. The authors read and approved the final manuscript.

Funding
Not applicable.

Availability of data and materials
The datasets used and/or analysed during the current study are available from the corresponding author on reasonable request.

Declarations

Competing interests
The authors declare that they have no competing interests.

Received: 17 January 2024 Accepted: 8 March 2024
Published online: 01 May 2024

References

Abdel-Ghaffar AM, Khalifa MA (1991) Importance of cable vibration in dynamics of cable-stayed bridges. J Eng Mech 117:2571–2589. https://doi.org/10.1061/(asce)0733-9399(1991)117:11(2571)
Beskhyroun S, Wegner LD, Sparling BF (2011) Integral resonant control scheme for cancelling human-induced vibrations in light-weight pedestrian structures. Struct Control Heal Monit. https://doi.org/10.1002/stc
Caracoglia L, Jones NP (2007) Damping of taut-cable systems: two dampers on a single stay. J Eng Mech 133:1050–1060. https://doi.org/10.1061/(asce)0733-9399(2007)133:10(1050)
Chen L, Sun L, Xu Y et al (2020) A comparative study of multi-mode cable vibration control using viscous and viscoelastic dampers through field tests on the Sutong bridge. Eng Struct 224:111226. https://doi.org/10.1016/J.ENGSTRUCT.2020.111226
Cu VH, Han B (2015) High-damping rubber damper for taut cable vibration reduction. Aust J Struct Eng 16:283–291. https://doi.org/10.1080/13287982.2015.1092690
de Sá Caetano E (2007) Cable vibrations in Cable-stayed bridges. IABSE
Di F, Sun L, Chen L (2021) Suppression of vortex-induced high-mode vibrations of a cable-damper system by an additional damper. https://doi.org/10.1016/j.engstruct.2021.112495
Di F, Sun L, Chen L (2020) Cable vibration control with internal and external dampers: theoretical analysis and field test validation. Smart Struct Syst 26:575–589. https://doi.org/10.12989/sss.2020.26.5.575
Duan Y, Ni YQ, Zhang H et al (2019a) Design formulas for vibration control of taut cables using passive MR dampers. Smart Struct Syst 23:521–536. https://doi.org/10.12989/sss.2019.23.6.521
Duan Y, Ni YQ, Zhang H et al (2019b) Design formulas for vibration control of taut cables using passive MR dampers. Smart Struct Syst 23:521–536. https://doi.org/10.12989/sss.2019.23.6.521
Fujino Y, Hoang N (2008) Design formulas for damping of a stay cable with a damper. J Struct Eng 134:269–278. https://doi.org/10.1061/(asce)0733-9445(2008)134:2(269)
Fujino Y, Kimura K, Tanaka H (2014) Wind resistant design of bridges in Japan: developments and practices. Springer Science and Business Media
Gu M (2009) On wind-rain induced vibration of cables of cable-stayed bridges based on quasi-steady assumption. J Wind Eng Ind Aerodyn 97:381–391. https://doi.org/10.1016/j.jweia.2009.05.004
Hoang N, Fujino Y (2008) Combined damping effect of two dampers on a stay cable. J Bridg Eng 13:299–303. https://doi.org/10.1061/(asce)1084-0702(2008)13:3(299)
Hung VD, Thao ND (2020a) A further study on stay cable galloping under dry weather condition BT - CIGOS 2019, innovation for sustainable infrastructure. In: Ha-Minh C, Dao D Van, Benboudjema F, et al. (eds). Springer Singapore, Singapore, p 191–196
Hung VD, Thao ND (2020b) A further study on stay cable galloping under dry weather condition. In: Lecture Notes in Civil Engineering. pp 191–196
Javanmardi A, Ghaedi K, Huang F et al (2022) Application of structural control systems for the cables of cable-stayed bridges: state-of-the-art and state-of-the-practice. Arch Comput Methods Eng 29:1611–1641
Kumarasena S, Jones NP, Irwin P, Taylor P (2005) Wind induced vibration of stay cables interim final report
Le LX, Katsuchi H, Yamada H (2020) Damping of cable with HDR damper accounting for restraint boundary conditions. J Bridg Eng 25:4020105. https://doi.org/10.1061/(asce)be.1943-5592.0001641
Liu Y, Xu YW, Wang ZH (2023) Free vibration of a taut cable with internal high damping rubber dampers and an external negative stiffness damper. J Low Freq Noise Vib Act Control 42:1018–1034. https://doi.org/10.1177/14613484221126365/ASSET/IMAGES/LARGE/10.1177_14613484221126365-FIG11.JPEG
Main JA (2002) Modelling the vibrations of a stay cable with attached damper. The Johns Hopkins University
Main JA, Jones NP (1967) influence of rubber bushings on stay-cable damper effectiveness. Angew Chemie Int Ed 6(11):951-952 5–24

Main JA, Jones NP (2002a) Free vibrations of taut cable with attached damper. I: linear viscous damper. J Eng Mech 128:1062–1071. https://doi.org/10.1061/(asce)0733-9399(2002)128:10(1062)
Main JA, Jones NP (2002b) Free vibrations of taut cable with attached damper. II: Nonlinear damper. J Eng Mech 128:1072–1081. https://doi.org/10.1061/(asce)0733-9399(2002)128:10(1072)
Main JA, Jones NP (2007) Vibration of tensioned beams with intermediate damper. I: Formulation, influence of damper location. J Eng Mech 133:369–378. https://doi.org/10.1061/(asce)0733-9399(2007)133:4(369)
Matsumoto M, Shirato H, Yagi T et al (2003) Field observation of the full-scale wind-induced cable vibration. J Wind Eng Ind Aerodyn 91:13–26. https://doi.org/10.1016/S0167-6105(02)00332-X
Matsumoto M, Yagi T, Shigemura Y, Tsushima D (2001) Vortex-induced cable vibration of cable-stayed bridges at high reduced wind velocity. J Wind Eng Ind Aerodyn 89:633–647. https://doi.org/10.1016/S0167-6105(01)00063-0
Nakamura A, Kasuga A, Arai H (1998) The effects of mechanical dampers on stay cables with high-damping rubber. Constr Build Mater 12:115–123. https://doi.org/10.1016/s0950-0618(97)00013-5
Nguyen DT, Vo DH (2020a) A study on combination of two friction dampers to control stayed-cable vibration under considering its bending stiffness BT - CIGOS 2019, innovation for sustainable infrastructure. In: Ha-Minh C, Dao D Van, Benboudjema F, et al. (eds). Springer Singapore, Singapore, p 87–92
Nguyen DT, Vo DH (2020b) A study on combination of two friction dampers to control stayed-cable vibration under considering its bending stiffness. In: Lecture Notes in Civil Engineering. 테크노프레스, p 87–92
Nguyen DT, Vo DH, Hai V, Haque MN (2022) Optimization of multiple helical fillets surface to suppress rain-wind vibration of stay cables: a wind tunnel investigation. Open Civ Eng J 16:1–12. https://doi.org/10.2174/18741495-v16-e2206270
Nguyen DT, Vo DH, Haque MN (2021) Theoretical investigation on the impact of two HDR dampers on first modal damping ratio of stay cable. Appl Sci 11:10985. https://doi.org/10.3390/app112210985
Nielsen SRK, Krenk S (2003) Whirling motion of a shallow cable with viscous dampers. J Sound Vib 265:417–435. https://doi.org/10.1016/S0022-460X(02)01455-4
Pacheco BM, Fujino Y, Sulekh A (1993) Estimation curve for modal damping in stay cables with viscous damper. J Struct Eng 119:1961–1979. https://doi.org/10.1061/(asce)0733-9445(1993)119:6(1961)
Sun L, Chen L (2015) Free vibrations of a taut cable with a general viscoelastic damper modeled by fractional derivatives. J Sound Vib 335:19–33. https://doi.org/10.1016/J.JSV.2014.09.016
Sun L, Huang H (2008) Design, implementation and measurement of cable dampers for large cable-stayed bridges. In: 17th Congress of IABSE. Creating and Renewing Urban StructuresInternational Association for Bridge and Structural Engineering. pp 242–243
Sun L, Xu Y, Chen L (2019) Damping effects of nonlinear dampers on a shallow cable. Eng Struct 196:109305. https://doi.org/10.1016/j.engstruct.2019.109305
Vo HD, Katsuchi H, Yamada H, Nishio M (2016) A wind tunnel study on control methods for cable dry-galloping. Front Struct Civ Eng 10:72–80. https://doi.org/10.1007/s11709-015-0309-7
Wang Z, Cheng Z, Wang H et al (2022) Damping of a stay cable with two eddy-current inertial mass dampers: theoretical analysis, experimental study, and parameter optimization. Struct Control Heal Monit 29:e3085. https://doi.org/10.1002/STC.3085
Wang XY, Ni YQ, Ko JM, Chen ZQ (2005) Optimal design of viscous dampers for multi-mode vibration control of bridge cables. Eng Struct 27:792–800. https://doi.org/10.1016/j.engstruct.2004.12.013
Zhou Y, Sun L (2006) Complex modal analysis of a taut cable with three-element Maxwell damper. Tongji Daxue Xuebao/Journal Tongji Univ 34:7–12

Publisher's Note